ELSEVIER

Polymer 43 (2002) 1897–1902

polymer

www.elsevier.com/locate/polymer

Liquid phase behavior and its effect on crystalline morphology in the extruded poly(ethylene terephthalate)/poly(ethylene-2,6-naphthalate) blend

Jong Kwan Lee[a], Kwang Hee Lee[a], Chang Hyung Lee[b,*]

[a]*Center for Advanced Functional Polymers, School of Chemical Science and Engineering, Inha University, Inchon 402-751, South Korea*
[b]*Department of Medical Devices and Radiation Health, Korea Food and Drug Administration, 5 Nokbeon-dong, Eunpyung-ku, Seoul, South Korea*

Received 1 May 2001; received in revised form 2 November 2001; accepted 7 November 2001

Abstract

Morphology in an extruded poly(ethylene terephthalate)/poly(ethylene-2,6-naphthalate) was investigated using time-resolved light scattering, optical microscope and small-angle X-ray scattering. During annealing at 280 °C, the domain structure via spinodal decomposition preceded, the transesterification followed, and then the transesterification between the two polyesters induced the dissolution of the liquid–liquid (L–L) phase separation, i.e. the homogenization. The annealed specimen for various time periods (t_s) at 280 °C was subjected to a temperature-drop to 120 °C for the isothermal crystallization and then the effects of liquid phase morphology on crystallization was investigated. With t_s, the H_v (cross-polarization) light scattering patterns exhibited the dramatic change from a four-leaf clover pattern with maximum intensity at azimuthal angle 45° (×-type scattering pattern) to a diffuse pattern of circular symmetry and then a four-leaf clover pattern with maximum intensity at azimuthal angles 0 and 90° (+-type scattering pattern). This suggests that the crystalline structure depends on the level of the block and/or random copolymer produced by the transesterification during annealing. The H_v scattering patterns reflected differences in the principle polarizability of the crystalline lamellae with respect to the spherulitic radius. On the other hand, the long period L_B, an average distance between two adjacent crystalline lamellae, increased with t_s at 280 °C. The dependence of L_B on t_s was explained by the change in the crystallization rate G.

Keywords: Phase behavior; Crystalline morphology; Blend

1. Introduction

Poly(ethylene terephthalate) (PET) and poly(ethylene-2,6-naphthalate) (PEN) are not miscible. In melt-compound, they inherently form two phases, resulting in a milky white bottle. The opacity of the bottles results from phase separation partly due to the L–L phase separation and partly due to different crystallization behaviors of the component polyesters.

During the melt-compounding of two polyesters, transesterification takes places [1–5]. The reaction leads to the formation of block copolyester species that enhance their miscibility, which in turn influences the gross structure through their phase behavior and crystallization. The transesterification in PET/PEN blend and its effect on miscibility have been reviewed by other researchers [4,5]. Okamoto and Kotaka [5] examined the competitive domain-structure development and homogenization during annealing in melt-extrudates of the PEN/PET blends. They found that the phase separation proceeded mainly through the demixing due to spinodal decomposition (SD), the transesterification followed, and then the multiblock copolymer species produced by transesterification induced the homogenization. The PEN/PET blend provides a nice opportunity to investigate the effects of the various liquid phase changes on crystalline morphology.

In this paper, we carried out time-resolved light scattering (TR-LS) studies to confirm L–L phase separation via SD and subsequent homogenization in PET/PEN blend, and investigated the effects of liquid phase morphology on crystallization.

2. Experimental

2.1. Blends procedures

Commercial PET and PEN produced by SKC Co. were used. The number average molecular weight, M_n, of PET

* Corresponding author. Tel.: +82-2-380-1756; fax: +82-2-351-3726.
E-mail address: c-hlee@kfda.go.kr (C.H. Lee).

0032-3861/02/$ - see front matter
PII: S0032-3861(01)00783-2

was 2.3×10^4, and the intrinsic viscosity of PEN in a mixed solvent of *p*-chlorophenol and tetrachloroethane (7/3 v/v) at 30 °C was 0.62 dl/g. After being dried in a vacuum oven at 150 °C for 24 h, PET and PEN were melt-mixed at 280 °C on a 30 mm co-rotating twin screw extruder (Werner Pfleiderer) at a speed of 200 rpm. The residence time for the melt-mixing was less than 1 min. After extrusion, the blend was quickly quenched in ice water to freeze the structure in the melt, and was then granulated to pellets. The composition of the PET/PEN blend was 50/50 by weight.

2.2. TR-LS and OM

A thin-layer specimen (ca. 15 μm thick) was prepared by pressing the blend pellets between two cover glasses at 280 °C. Immediately after melt-pressing, the specimen was quickly transferred into a hot stage on light scattering photometer equipped with a charge-coupled device (CCD) camera [6], and the behavior of the L–L phase separation and homogenization was investigated. To confirm these phenomena, the final morphology of the crystallized specimen at 120 °C after t_s was also observed under an optical microscope (OM). The time t_s is the time spent for annealing at 280 °C above the crystal melting temperatures of PET and PEN.

The L–L phase-separated and homogenized specimen for t_s was rapidly transferred into a light scattering hot stage set at 120 °C for the isothermal crystallization and then the effect of L–L phase separation on crystallization was investigated. At 120 °C, only PET crystallizes and PEN remains amorphous. A polarized He–Ne gas laser of 632.8 nm wavelength was applied to the film specimen. We employed the V_v geometry in which the optical axis of the analyzer was set parallel to that of the analyzer. The crystallization kinetics were also studied by TR-LS employing the H_v geometry with a perpendicular set of the two optical axes.

2.3. Small angle X-ray measurements

The pellets were annealed between metal plates at 280 °C for $t_s = 1$, 3 and 7 min. The annealed specimen was rapidly transferred into another hot chamber set at 120 °C at which only PET crystallized. This crystallized specimen was used for small-angle X-ray scattering (SAXS).

The X-ray beam was from synchrotron radiation; beam line 4C2 at Pohang Accelerator Laboratory, Pohang, South Korea. The storage ring was operated at an energy level of 2 GeV. The SAXS employs a point focusing optics with an Si double crystal monochromator followed by a bent cylindrical mirror. The incident beam intensity of 0.149 nm wavelength was monitored by an ionization chamber for the correction of minor decrease in the primary beam intensity during the measurement. The scattering intensity, *I*, was corrected for background scattering. The correction for smearing effect by the finite cross-section of the incident beam was not necessary for the optics of SAXS with point focusing.

3. Results and discussion

3.1. L–L phase separation and homogenization

The extruded PET/PEN blend was held at 280 °C and the behavior of L–L phase separation and homogenization was investigated by TR-LS. Fig. 1(a) shows a typical example of time evolution of the one-dimensional V_v scattering profile for $t_s < 3$ min, in which the scattering vector q is defined by $q = (4\pi/\lambda')\sin(\theta/2)$, where λ' is the wavelength of light in the specimen and θ is the scattering angle. The peak intensity I_m increases with t_s, and its position, q_m, shifts to smaller angles, implying that the L–L phase separation proceeds via SD mechanism.

The change of the scattering profiles for $t_s > 5$ min is seen in Fig. 1(b). The q_m further shifts toward much smaller angles in the beamstop area and the scattering intensity decreases with t_s. At $t_s = 15$ min, the intensity becomes very weak and shows hardly q-dependence, suggesting that the phase homogenization is complete in the blend.

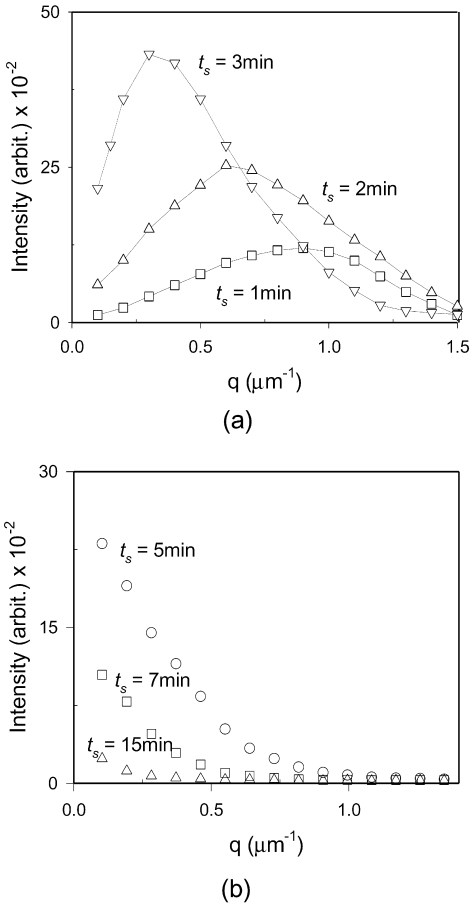

Fig. 1. Changes in V_v light scattering profile of a 50/50 PET/PEN blend (a) during the earlier stage of annealing ($t_s < 3$ min) at 280 °C and (b) during the later stage of annealing ($t_s > 5$ min) at 280 °C.

This scattering feature due to L–L phase separation and subsequent homogenization during annealing is consistent with the results of the investigation by Okamoto and Kotaka [5]. They concluded that the phase separation proceeded mainly through demixing due to SD, the transesterification followed, and then the multiblock copolymer species produced by transesterification induced the homogenization.

A supplemental evidence of L–L phase separation and homogenization formed at 280 °C was given by observing a morphology crystallized at 120 °C. At 120 °C, L–L phase separation rate may be negligible, whereas the crystallization rate of PET is high. Note that the crystallization temperature 120 °C is below the glass transition temperature T_g of PEN. In such a case, it is well known that the liquid phase morphology formed before crystallization is preserved during the crystallization process [7,8]. Fig. 2 shows an optical micrograph of a blend crystallized at 120 °C after $t_s = 1$, 3, 10 and 15 min. The white regions may be the PET-rich phases, since the refractive index of the PET (1.57) [9] is lower than that of the PEN (1.65) [10]. As expected, a highly interconnected phase with unique periodicity is seen in Fig. 2(a). Connectivity of phases is an important morphological feature of SD. At the late stage, the phase connectivity seems to grow in size while maintaining their connectivity (Fig. 2(b) and (c)). Finally, the blend shows a homogeneous mixture, suggesting that the blend is homogenized (Fig. 2(d)).

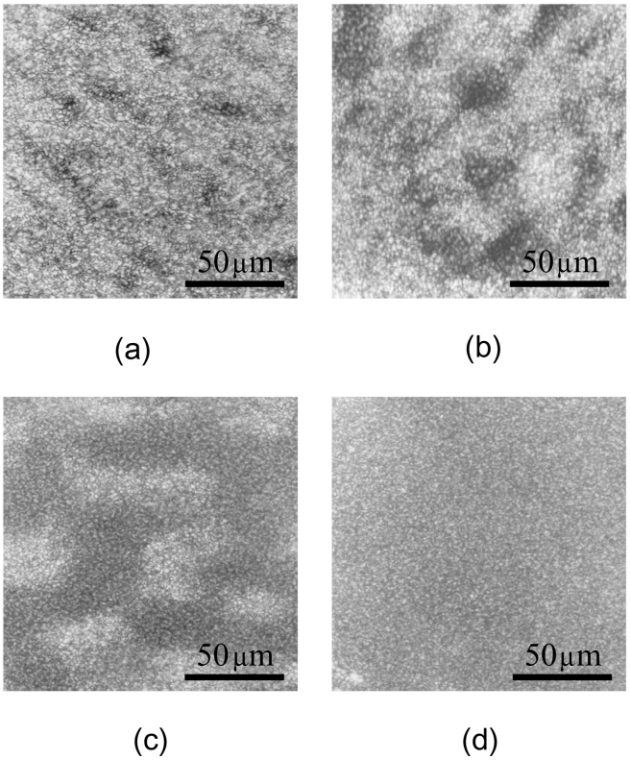

Fig. 2. Optical micrographs of a 50/50 PET/PEN blend crystallized at 120 °C after (a) $t_s = 1$ min; (b) $t_s = 3$ min; (c) $t_s = 10$ min; (d) $t_s = 15$ min at 280 °C.

From the above results, it can be known that the structure development of the extruded PET/PEN blend in the early stage of annealing at 280 °C is dominated by the SD mechanism. A possible explanation for this phase behavior may be given as follows: under the high shear rate in the extruder, phase diagram elevated over the barrel temperature and one phase region becomes wide. Thus, the blend could be done in a wide temperature window for dissolution to get a homogeneous mixture. However, once the melt is extruded out from nozzle, the shear rate turns out to be zero and lower critical solution temperature (LCST) will immediately go down to the state without shear so that the SD will proceed until the system is cooled down to crystallization.

3.2. Effect of L–L phase separation and homogenization on crystalline structure

3.2.1. Structure on the spherulite level

The specimens proceeded by L–L phase-separation and homogenization for t_s were allowed to crystallize by rapid temperature drop to a light scattering hot stage set at 120 °C for the isothermal crystallization. To discuss the crystallization, it is convenient to employ the integrated intensity, invariant Q, defined by [11]

$$Q = \int_0^\infty I(q) q^2 \, \mathrm{d}q \tag{1}$$

The time variation of the invariant in the H_v mode (parallel polarization), Q_{H_v}, is shown in Fig. 3. To discuss the effect of the L–L phase separation structure on crystallization kinetics, one can use the TR-LS. Q_{H_v} can be described by

$$Q_{H_v} \propto \langle \delta^2 \rangle = \phi_s \delta_s^2 \tag{2}$$

where $\langle \delta^2 \rangle$ is the mean-square anisotropy, ϕ_s, the volume fraction of spherulite and δ_s, the spherulite anisotropy [11]. At the early stage of crystallization, Q_{H_v} is assumed to be proportional to the volume fraction of spherulite so that the

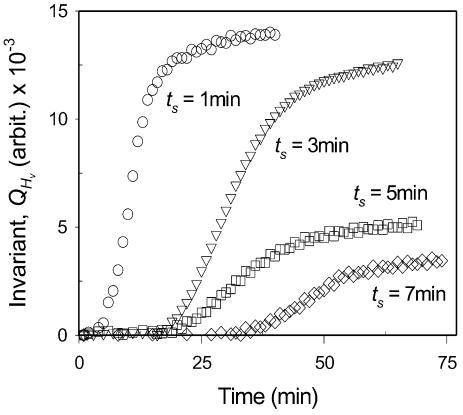

Fig. 3. Time variation of the invariant Q_{H_v} in a 50/50 PET/PEN blend crystallized at 120 °C after (a) $t_s = 1$ min; (b) $t_s = 3$ min; (c) $t_s = 5$ min; (d) $t_s = 7$ min at 280 °C.

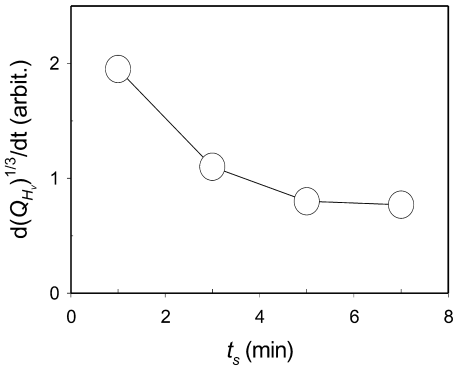

Fig. 4. Change of G with t_s.

linear growth rate of spherulite G is given by

$$G \propto \mathrm{d}(Q_{H_v})^{1/3}/\mathrm{d}t \tag{3}$$

Hence, one can estimate G from the initial slope of the time variation of $(Q_{H_v})^{1/3}$. The values of G estimated by Eq. (3) are shown as a function of t_s in Fig. 4. G decreases with t_s. This may come from the increase in the amount of PEN/PET block and/or random copolymer species. The increase in the amount of PEN/PET block and/or random copolymer species with t_s seems to originate from transesterification of the two polyesters during SD process at 280 °C before crystallization; as L–L phase separation via SD proceeds, the transesterification between the two polyesters takes place, and the product block copolymer increases. With increasing amount of PEN/PET block and/or random copolymer species, the T_g in PET molecules increases. Note that T_g in PEN is higher than that in PET. Higher T_g decreases diffusion coefficient so that crystallization rate is reduced. Crystallization rate consists of nucleation rate and diffusion rate. The existence of PEN/PET block and/or random copolymer species may retard the crystallization rate and thereby the crystallization rate with t_s can be decreased.

The effect of L–L phase separation and homogenization on spherulite level was investigated by H_v light scattering patterns. Fig. 5 shows H_v scattering patterns for the specimen annealed for $t_s = 1$, 5 and 15 min and subsequently crystallized isothermally at 120 °C. The scattering patterns change the shape from a four-leaf clover pattern with maximum intensity at azimuthal angle 45° (×-type scattering pattern) to a diffuse pattern of circular symmetry and then a four-leaf clover pattern with maximum intensity at azimuthal angles 0 and 90° (+-type scattering pattern).

The ×-type scattering pattern in Fig. 5(a) is typical for negatively birefringent spherulite whose tangential polarizability component is larger than the radial component. Actually, the spherulites with negative birefringence were observed under the polarized microscopy. The birefringence

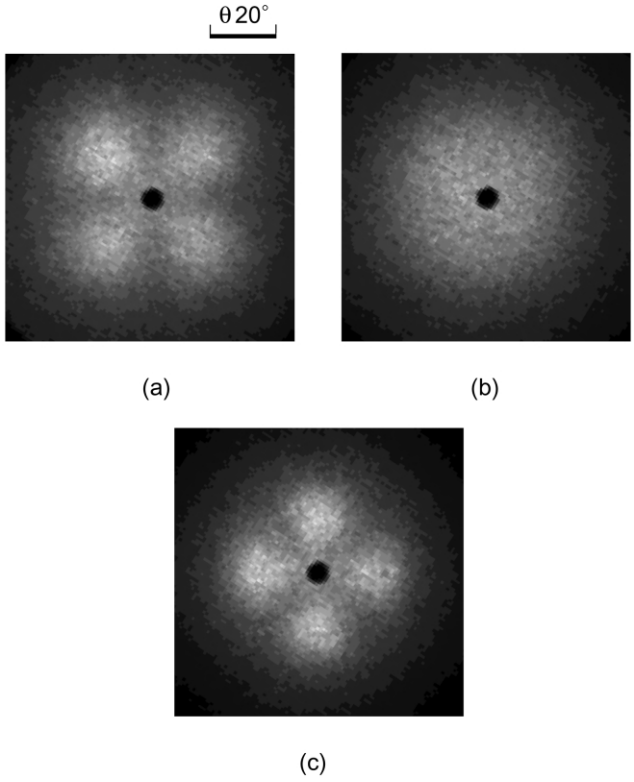

Fig. 5. Changes in H_v light scattering pattern of a 50/50 PET/PEN blend crystallized at 120 °C after (a) $t_s = 1$ min; (b) $t_s = 5$ min; (c) $t_s = 15$ min at 280 °C.

of a spherulite is given by [12]

$$\Delta n = n_r - n_t = \left(\frac{3f-1}{2}\right)(n_c - n_a) \tag{4}$$

where f is the fraction of tangential lamellae, n_r and n_t are the average radial and tangential refractive indices, respectively, and n_c and n_a are the principal refractive indexes along the a- and c-axes of a crystal, respectively. The negative birefringence ($\Delta n < 0$) suggests that f is smaller than 1/3, implying a significant amount of the radial lamellae. Therefore, the pattern in Fig. 5(a) can be interpreted by a significant amount of the radial lamellae. The Δn increases with increasing fraction of radial lamellae.

The circular symmetric pattern in Fig. 5(b) means no azimuthal angle dependence of the scattered light pattern. The H_v scattering pattern is dependent on the internal anisotropy of the spherulite which reflects the order of crystalline lamellae orientation within the spherulite. According to Stein and Chu [13], the disorder parameter is described by the orientation angle fluctuation of the optic axis within a spherulite. They suggested by the model calculation of the scattering patterns that the large disorder results in the broad H_v scattering pattern, i.e. as the disorder parameter increases, the azimuthal dependence of the scattering pattern becomes less and the scattering pattern shows a diffuse pattern of circular symmetry. Then the pattern in

Fig. 5(b) suggests the disordered arrangement of the crystalline lamellae within the spherulite.

Fig. 5(c) displays a scattering pattern characteristic of spherulite whose major optical axis, i.e. lamellar principle axis lies at an angle close to 45° with respect to the spherulite radius, implying a significant amount of the fraction of lamellae at an angle close to 45° with respect to the radial direction. Then, the appearance of the +-type four-leaf clover pattern is ascribed to the high fraction of lamellae at an angle close to 45°.

One may mention two possibilities about the dramatic change of the scattering patterns: one is the L–L phase separation formed in the melt-liquid state and the other is the amount of PEN/PET block and/or random copolymer species produced by transesterification. The latter possibility seems to be more realistic, as the liquid phase morphology such as SD structure slightly affect the spherulite structure for the rapid crystallization rate and slow L–L phase separation rate [7,8]. In addition, the ×-type, +-type, and circular symmetry-type scattering pattern has been reported in segmented polyether–polyester block copolymer [14,15]. Therefore, one may conclude that the change in the principle polarizability of the spherulite associates with copolymer species is formed by trans-esterification rather than the L–L phase separation before crystallization.

3.2.2. Structure on the crystalline lamellae level

Fig. 6 shows the SAXS profiles. From the peak position of the SAXS profiles, the long period L_B can be obtained by Bragg equation. Other parameters related to lamellar morphology can be estimated from the correlation function $K_1(z)$, which is given by the Fourier transform of the scattering intensity $I(q)$ [16]:

$$K_1(z) = \int_0^\infty q^2 I(q)\cos(qz)\mathrm{d}q \tag{5}$$

where z is the coordinate along which the electron density distribution is measured. The approach to estimate variables related to lamellar morphology is illustrated in Fig. 7, which shows a typical $K_1(z)$ obtained for $t_s = 1$ min. The

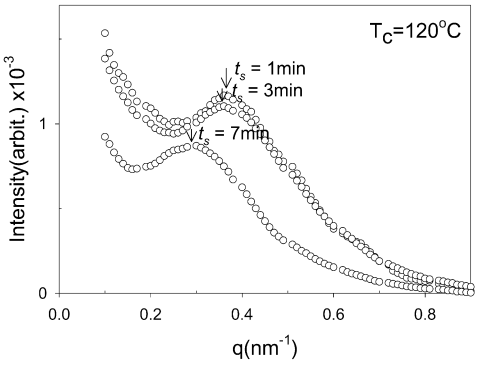

Fig. 6. SAXS profiles of a 50/50 PET/PEN blend crystallized at 120 °C after (a) $t_s = 1$ min; (b) $t_s = 3$ min; (c) $t_s = 7$ min at 280 °C.

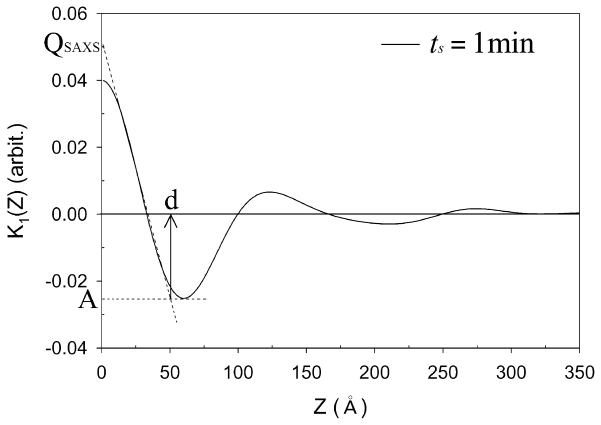

Fig. 7. Correlation function of a 50/50 PET/PEN blend crystallized at 120 °C after $t_s = 1$ min at 280 °C.

crystalline lamellar thickness may be calculated from the baseline procedure [16]. The extrapolation of the initial slope for the $K_1(z)$ intersects the base line $K_1(z) = -A$ at $z = d$, the average thickness of the crystalline region. Here, the base line is the horizontal line for the plateau region of the first minimum of $K_1(z)$ and the slope $\mathrm{d}K_1(z)/\mathrm{d}z$ is given by

$$\mathrm{d}K_1(z)/\mathrm{d}z = -(Q_{\mathrm{SAXS}} + A)/d \tag{6}$$

where Q_{SAXS} is the invariant which is obtained by extrapolating $K_1(z)$ to $z = 0$. The morphological parameters obtained by SAXS are shown as a function of t_s in Fig. 8.

The long period (L_B) increases with t_s. Taking account of constant lamellar thickness (d), it may suggest that an amount of impurity entrapped between PET crystalline lamellae increases with t_s. The increased impurity between PET crystalline lamellae results in an increase in periodicity L_B with t_s. The concentration of the impurity between lamellae can be caused by rejection of non-crystalline component on the thickness scale of lamellae during crystallization.

To discuss the effect on L_B of the rejection of non-crystalline component, it may be interesting to employ the

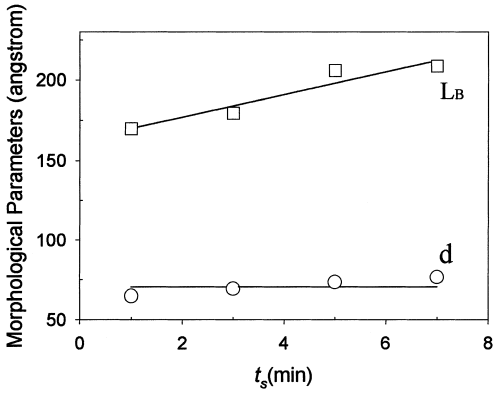

Fig. 8. Morphological parameters by SAXS as a function of t_s: L_B, the long period by the Bragg equation; d, lamellar thickness by the correlation function method.

Keith–Padden's δ parameter, which describes a scale in exclusion distance of impurities [17,18]:

$$\delta = D/G \tag{7}$$

where D and G are the diffusion rate of impurity and the growth rate of the crystalline component, respectively. When the value of δ is comparable with the interlamellar distance, the rejected non-crystalline impurity may reside between lamellae. Such a rejection is often found in high crystallization rate or in low D. If G is larger or D smaller, then D/G may be sufficiently small so that the rejected impurity resides between crystalline lamellae. Interlamellar rejection of impurity results in an increase of periodicity L_B (i.e. the sum of the lamellar thickness and the amorphous layer between the lamellae). In Fig. 8, L_B as a measure of δ increases with t_s. Thus, combining the G results in Fig. 4 with Eq. (7), one may conclude that the increase in L_B contributes to the decrease in G with t_s.

4. Conclusions

The results of morphology analysis demonstrated that the L–L phase separation during annealing of the melt-extruded PET/PEN blend preceded, the transesterification followed, and then the homogenization occurred.

The effect of liquid phase structure on the spherulite morphology produced by subsequent crystallization was discussed. With annealing time before crystallization, the principle polarizability of the crystalline lamellae with respect to the spherulitic radius change from the tangential polarizability of the spherulite to the random polarizability without specific direction and then to the polarizability at an angle close to 45° with respect to the radial direction. This change related to the increase in the block and/or random copolymer produced by the transesterification during annealing. By a series of crystalline morphological parameters by SAXS, it was shown that the crystallization rate decreased with annealing time before crystallization and its decrease induced the larger long period.

Acknowledgements

This research was supported by the Center for Advanced Functional Polymers. Synchrotron SAXS experiments were performed at the Pohang Light Source (4C1 beam line) in Korea, which was supported by MOST and Pohang Iron and Steel Co. (POSCO).

References

[1] Backson SCE, Kenwright AM, Richards RW. Polymer 1995;36:1991.
[2] Kugler J, Gilmer JW, Wiswe D, Zachmann HG, Hahn K, Fischer F. Macromolecules 1987;20:1116.
[3] Benoit HC, Fischer EW, Zachmann HG. Polymer 1989;30:379.
[4] Stewart ME, Cox AJ, Naylor DM. Polymer 1993;34:4060.
[5] Okamoto M, Kotaka T. Polymer 1997;38:1357.
[6] Lee CH, Saito H, Inoue T. Macromolecules 1995;28:8096.
[7] Inaba N, Sato K, Suzuki S, Hashimoto T. Macromolecules 1986;19:1690.
[8] Inaba N, Yamada T, Suzuki S, Hashimoto T. Macromolecules 1988;21:407.
[9] Brandrup J, Immergut EH, Grulke EA. Polymer handbook. New York: Wiley/Interscience, 1999. Chapter 6.
[10] Cakmak M, Wang YD, Simhambhatla M. Polymer 1990;30:721.
[11] Koberstein T, Russell TP, Stein RS. J Polym Sci, Polym Phys Ed 1979;17:1719.
[12] Meeten GH. Optical properties of polymers. London: Elsevier Applied Science Publishers, 1986.
[13] Stein RS, Chu W. J Polym Sci A-2 1970;8:1137.
[14] Lilaonitkul A, West JC, Cooper SL. J Macromol Sci Phys B 1976;12:563.
[15] Matsuo M, Geshi K, Moriyama A, Sawatari C. Macromolecules 1982;15:193.
[16] Strobl GR, Schneider MJ, Voigt-Martin IG. J Polym Sci, Polym Phys Ed 1980;18:1361.
[17] Keith HD, Padden Jr FJ. J Appl Phys 1964;35:1270.
[18] Keith HD, Padden Jr FJ. J Appl Phys 1963;34:2409.